NRIAG JOURNAL OF ASTRONOMY AND GEOPHYSICS
2020, VOL. 9, NO. 1, 402–419
https://doi.org/10.1080/20909977.2020.1755479

Characteristics of the simulated pollutants and atmospheric conditions over Egypt

A. Saber, H. Abdel Basset, Mostafa Morsy, F. M. El-Hussainy and M. M. Eid

Astronomy and Meteorology Department, Faculty of Science, Al-Azhar University, Cairo, Egypt

ABSTRACT

In this paper the integrated chemistry-climate model (RegCM4-CHEM) was used to study the characteristics of the simulated pollutants and atmospheric conditions over Egypt with a focus on the Nile Delta (ND) region. The densely populated ND region is known for its severe air quality issues driven by high levels of anthropogenic pollution in conjunction with natural sources such as dust, and agricultural burning events. The data used in our study is from Monitoring Atmospheric Composition and Climate reanalysis data (2003–2010) and from the RegCM4-CHEM model simulation (2001–2010) over Egypt. It is found that surface ozone (O_3) has higher values during the period from May to September that indicates their sensitivity to temperature and sinking air above the subtropical high pressure during these hot months. Higher values of carbon monoxide (CO) occur in winter associated with the largest amounts of fuel burning in winter. The higher values of formaldehyde (HCHO) occur in summer associated with high temperatures and an abundance of OH (hydroxyl radical). The higher values of NOy appear in summer months, September and October in the layer between 1000 and 300 hPa, it is in the upper layer is generally greater than in the middle because it contains nitrogen oxide (NOx), which regarded as a catalyst in O_3 loss and production.

ARTICLE HISTORY
Received 4 March 2020
Revised 25 March 2020
Accepted 3 April 2020

KEYWORDS
Egyptian air pollution; pollutants transport; RegCM4-CHEM model; ozone and VOCs; air Quality

1. Introduction

The pollution is undoubtedly one of the greatest problems facing the world, especially air pollution. Pollutants play an important role in changing atmospheric chemical composition and the climate system (IPCC 2013). Currently, poor air quality is one of the most pressing problems that have very harmful impacts on health and the environment especially in urban areas (NRC 2001; EEA 2015). These pollutants have harmful effects on humans, animals, plants and constructions. The sources of air pollution can be classified into natural, like volcanic eruptions and natural decomposition of organic substances or forest, and anthropogenic, due to the global population and human activities increasing (Popescu and Ionel 2010). Anthropogenic emissions are recognised as one of the greatest contributors to the increase of atmospheric pollution and its concentrations. In addition, the atmospheric phenomena that occur on different spatial scales also contribute to environmental damages increasing (Miranda et al. 2016). The atmospheric pollutants are gaseous and suspensions of liquid, solid, or mixed particles with highly variable chemical composition and size distribution (Putaud et al. 2010). These suspended matters named aerosols and involve both organic and inorganic components. The global anthropogenic aerosols concentrations have markedly increased since the industrial revolution beginning due to human activity growth (Wang et al. 2017). Increasing air pollution is mainly caused by high levels of ozone (O_3), carbon monoxide (CO), nitrogen oxides (NO_x = NO + NO_2), sulphur dioxide (SO_2), particulate matter (PM) and non-methane volatile organic compounds (VOCs) in the atmosphere. The primary pollutants (as SO_x and NO_x) are emitted directly into the atmosphere, while the secondary pollutants are produced from the chemical reactions of primary pollutants as tropospheric ozone and acids (Lelieveld et al. 2019; EPA 2018). Most of the primary reactive gas O_3, CO, formaldehyde (HCHO), NOx and SO_2 play major roles in the atmospheric chemistry with the presence of OH (hydroxyl group) radicals (Steiner et al. 2014). Furthermore, the VOCs and NO_y have important impacts on the human health and reactions in the atmosphere that leads to produce many very harmful secondary pollutants and affect the levels of O_3 (Shalaby et al. 2012; Steiner et al. 2014; EEA 2015; WHO 2018). The Egyptian Nile Delta (ND), especially the cities of Greater Cairo (GC) and the surrounding areas, is one from many regions in the world that suffer from air pollution problems. The GC region in Egypt is one of the most densely populated areas with a population of more than 15 million people (CAPMAS 2017). The massive motorised traffic as well as several factories located in or around the GC play a major role in increasing air pollution in the region. Additionally, the black cloud phenomenon caused by

CONTACT A. Saber astmet2011@azhar.edu.eg Astronomy and Meteorology Department, Faculty of Science, Al-Azhar University, Cairo 11884, Egypt

smoke advection generated from burning rice straw after harvest in ND was observed in GC during October and November when temperature inversions helped exacerbate the situation (World Bank 2013). Prior studies describe that black cloud over ND and its vicinity may affect regional climate through radiation scattering or absorption (Haywood et al. 1999; Herman and Celarier 1997; Robaa 2004; El-Metwally et al. 2008; Fetouh et al. 2013) and explained that black cloud may influence plant growth in ND by changing the amount of radiation available for photosynthesis. Other studies (Abdul-Wahab and Bouhamra 2004; El-Metwally et al. 2011) suggested that the aerosols pre-sources can be classified into three main sections produced by (1) the daily activities, (2) the agricultural sector (Eid et al. 2014; Saber et al. 2017) in the ND and (3) desert dust. Also, higher aerosol concentrations were found in July due to the high stability of the atmospheric conditions. Wheida et al. (2017) showed that the peaks of the sharp aerosol concentration are mostly due to the advection of dust towards the GC from surrounding deserts or the burning of agricultural waste carbonaceous products in the ND.

The regional climate and chemistry models play an important role to simulate and predict the aerosols emissions and concentrations and air quality over any domain, where RegCM4-CHEM is one of these models maintained by the International Centre for Theoretical Physics (ICTP). Solmon et al. (2016) used RegCM4-CHEM over the domain from northern Europe to southern sub-tropical Africa and validates the model results against surface concentrations and aerosol optical depth (AOD) datasets for the winter and summer of 2000. The model validation shows that it was able to simulate the regional patterns and seasonality of the pollutants and aerosols over their study area, with high accuracy. Also Shalaby et al. (2012) proved that the RegCM4-CHEM model can simulate the O_3 event of August 2003 as well as its long term seasonal cycle, with an overestimation of concentration in the non-event years and shows the ability use RegCM4-CHEM in aerosols and pollutants simulation in general. Steiner et al. (2014) moreover used the RegCM4-CHEM over Northern Africa and the Mediterranean, with a focus on the GC region. These studies applied a two ways interface between the atmospheric chemistry and dynamics, and study the major relation between atmospheric chemistry and climate, and test the RegCM4-CHEM in the simulation of pollutants and aerosols especially seasonal cycle of O_3. Mostafa et al. (2019) used the RegCM4-CHEM model to simulate the air quality over the GC domain during three years (2010–2012) for O_3, CO, NO_2, SO_2, PM and other variables to test its ability to simulate the measured pollutant concentrations. Their study use observed data at various sites in GC to compare with RegCM4-CHEM to validate it. Calculation of the bias between the model results and the measured data was used to evaluate the model performance and shows the ability to exhaust the RegCM4-CHEM in air quality simulations over the GC region.

The main objectives of this work are to assess the ability of RegCM4-CHEM to simulate atmospheric conditions (temperature, relative humidity and wind) and concentration of pollutants (O_3, CO, CH_4, HCHO, NO_x and SO_2). In addition, an analysis and characteristics of some important pollutants (O_3, CO, HCHO, VOCs and NO_y (NO_x + HNO_3 + PAN (peroxyacyl nitrate)) and their transport along with chose weather parameters. As well as determine the role of the atmospheric condition in pollutants transport over Egypt and the ND regions.

2. Data and methodology

2.1. Data

To achieve the purposes of this study, four different data types are used: six hourly with 0.5° × 0.5° horizontal resolution data for concentrations of ozone O_3, CO, CH_4, nitrogen oxides NO_x, HCHO and SO_2 during the period 2003–2010 at 11 pressure levels (1000, 925, 850, 700, 500, 400, 300, 250, 200, 150 and 100 hPa) were taken from the Monitoring Atmospheric Composition and Climate (MACC) reanalysis dataset. MACC is a research project with the aim of establishing the core global and regional atmospheric environmental services for the European GMES (Global Monitoring for Environment and Security) initiative (Schultz et al. 2005; Inness et al. 2013). MACC was based on the global model and data assimilation system from the European Centre for Medium-Range Weather Forecasts (ECMWF) Integrated Forecast System (IFS). This data type was used for the evaluation of RegCM4-CHEM for environmental pollution concentration simulation. Six hourly with 0.5° × 0.5° horizontal resolution data for temperature (T) in °K, meridional and zonal wind components (u-eastward and v-northward) in ms^{-1}, and Relative humidity (RH) in % during the period 2001–2010 were obtained from ECMWF (ERA-Interim) reanalysis dataset. This data type was used for the assessment of RegCM4-CHEM for meteorological variables simulation. The RegCM4-CHEM initial and lateral boundary atmospheric conditions (ICBC) were downloaded from the National Center for Environmental Prediction (NCEP) and the National Center for Atmospheric Research (NCAR) Reanalysis Project-2 (NNRP2) global datasets during the period 2001–2010 with 2.5° × 2.5° spatial grid every 6 hours at the standard 17 pressure levels. The RegCM4-CHEM chemistry boundary conditions were collected as monthly averages of OH and CO chemical production fields from the Model for Ozone and Related chemical tracers version-4 (MOZART-4), which is an offline global chemical transport model for the

tropospheric studies (Beekmann and Vautard 2010; Emmons et al. 2010).

2.2. Model description, settings, and configured domain

The RegCM4-CHEM is the ICTP (International Centre for Theoretical Physics) online-integrated Regional Climate Model (RegCM) coupled with the condensed gas-phase chemistry (atmospheric chemical transport model) which is based on the Carbon Bond Mechanism-Z (CBM-Z) (Zaveri and Peters 1999). The RegCM4-CHEM is a hydrostatic, sigma-coordinate following model (Zaveri and Peters 1999; Elguindi et al. 2014), which can be applied to any interesting region of the globe with high resolution for regional climate studies (Giorgi et al. 2012; Elguindi et al. 2014). This model has undergone many updates to be widely used in climate simulation and pollution. The physics (dynamics) component of the latest version of RegCM (version 4) has (not) changed considerably from that of the prior versions. During a series of developments the RegCM has represented aerosols and chemistry modules (Sylla et al. 2009). Zakey et al. (2006) then added a 4-bin desert dust size module. The dust generation scheme accounts for sub-grid emissions by different types of soil, and the distributions of soil texture have been updated according to Laurent et al. (2008), and the distribution of dust size emissions now can be handle according to Kok (2011). The tracer version of RegCM4-CHEM is employed in this study to simulate the climate and pollution transport during the period of 10 years (1 January 2001 to 31 December 2010) preceded by two months as model spin-up period. The simulation was performed on a Rotated Mercator conformal projection single domain centred on 27.5° N and 35.0° E and extended between latitudes 10.4°–44.6° N and longitudes 15.1° E–58.0° E with a horizontal resolution of 50 km and 18 vertical sigma levels. An adaptive time step of 30 seconds has been set for the model iteration which integrated every 6 hours as the model output. To ignore the relaxation zone around the simulation domain, the regrid method was applied to the model output, where the model domain becomes 17.25°–37.75° N and 17.25°–52.75° E (Figure 1). In this study we will select the Egypt domain with the coordinates 21°–34°N and 24°–38° E (selected domain). Whereas the high pollutant concentrations are related to the sources of their emission, the delta in Egypt as the most source of the pollution, and the reasons were previously explained. Accordingly, we have focused on our study on a large part of the delta, whose coordinates 29.5°–31.25° N and 30.25°–31.75° E (study area) (Figure 1).

The RegCM4-CHEM has various options for physics and chemistry parameterisation schemes. For this study, the radiation scheme used is the community climate model CCM3 (Grell 2011), the cumulus scheme is mass-flux (Kiehl et al. 1996), the convection scheme is Grell et al. (2005) and the planetary boundary layer (PBL) scheme is Holtslag and Boville (1993). Moreover, the utilised chemistry simulation type is DCCB with activation of the CBM-Z (gas phase and sulphate) chemical tracer, DUST (4 dust bins scheme) and CARB (4 species black/anthropic carbon) (Nenes et al. 1998; Fountoukis and Nenes 2007). The Biosphere-Atmosphere Transfer Scheme (BATS) was used as the surface layer of land-atmosphere interactions (Dickinson et al. 2007). The photochemical CBM-Z was used as the chemistry routines, which based on the Tropospheric Ultraviolet-Visible Model (TUVM) scheme developed by Madronich and Flocke (1999). The model used the Community Land Model 4 (CLM4) for dry deposition (Wesely 1989) and the MOZART global model (Emmons et al. 2010) for wet deposition.

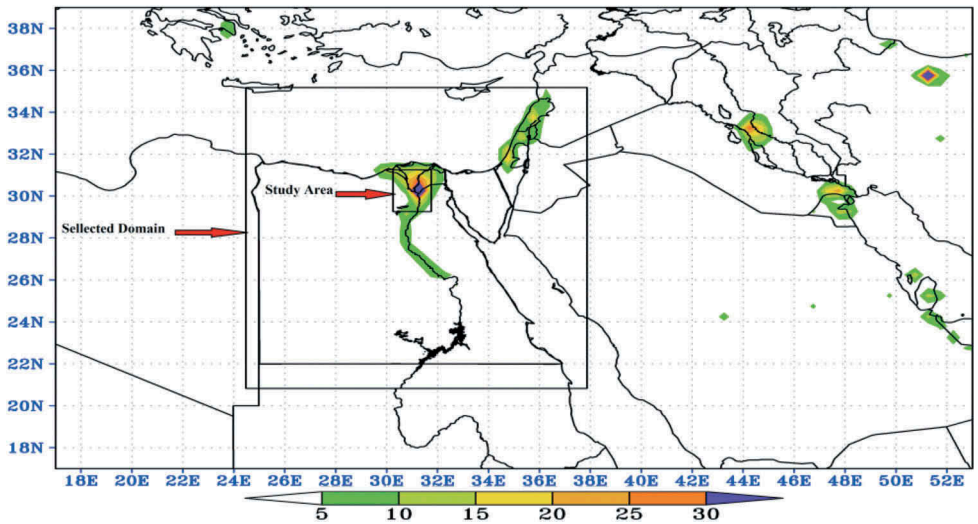

Figure 1. CO emissions as a sample for the main source of emissions.

3. Results and discussion

In this section the RegCM4-CHEM validation for both climate and pollution simulation against the MACC reanalysis dataset will be discussed in different subsections over a wide domain and focusing on the Greater Cairo (GC) area.

3.1. RegCM4-CHEM validation

This section presents and discusses the comparison between RegCM4-CHEM simulation and MACC reanalysis data for the temporal (seasonal and annual) variation of the selected 6 pollutants (O_3, CO, CH_4, HCHO, NO_X and SO_2) concentration and 4 meteorological variables (T, RH, wind speed and wind direction) as an area average over the interested area (Nile Delta and Cairo).

3.2. Climatology monthly mean variation

The monthly variation of the meteorological variables from RegCM4-CHEM resemble the MACC reanalysis, but with some biases in their values (Figure 2). Figure 2 (a) illustrates that there is a good agreement between the monthly mean values of reanalysis (MACC) and simulated (RegCM4-CHEM) temperature, where the simulated temperature is slightly overestimating the reanalysis throughout all months of the year with the higher difference in summer months (May–August). Although the time series of the reanalysis monthly mean of RH have the same behaviour as the corresponding simulated, there is a considerable difference between their values (Figure 2(b)). The difference increases during the period from March to October with a maximum in May and June. Also, the lower value of the reanalysis RH (in May) is one month earlier than the simulated (June). Figure 2 (c) illustrates that there is a good agreement between the monthly mean values of reanalysis and simulated zonal wind (u), where the simulated zonal wind is underestimating the reanalysis throughout all months of the year with the higher difference in spring and autumn. A good agreement appears between the monthly mean values of reanalysis and simulated meridional wind (v), and the simulated meridional wind is overestimating the reanalysis throughout all months except during the summer months (Figure 2(b)).

The seasonal variation of the simulated pollutants concentration resembles that of the observation, but with some biases in the values (Figure 3). It is clear that the time series of monthly mean values of the simulated O_3 concentrations have the same behaviour of the corresponding observed, and the higher values occur during the summer months while the lower values appear during the winter months (Figure 3(a)). Generally, the simulated O_3 concentrations are overestimating the observed throughout all months of the year. It is clear that the simulated monthly values of O_3 ranged between 45 and 64 μg/kg, while the observed O_3 ranged between 37 and 58 μg/kg. The small differences between the simulated and observed appear in May and June.

The very good agreement appears between the monthly mean values of observed and simulated CO concentrations throughout all months of the year except in October, November and December where the simulated CO concentrations are slightly underestimating the observed (Figure 3(b)). The higher value of simulated CO is 168 μg/kg in February and the lower values appear in July (143 μg/kg), while the higher values of observed CO concentration is 280 μg/kg in February and the lower values are 16 μg/kg in July also. Figure 3(c) illustrates that

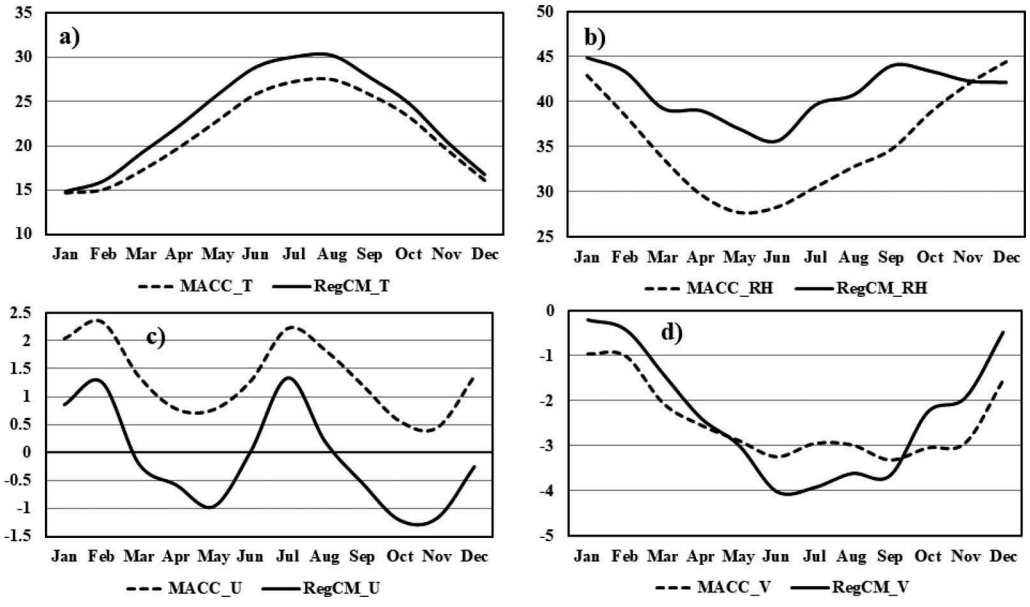

Figure 2. Annual cycle of MACC, (dashed line) and RegCM4-CHEM, (solid line): (a) *T*, (b) RH, (c) u-wind wind and (d) v-wind near-surface area average during 2003–2010.

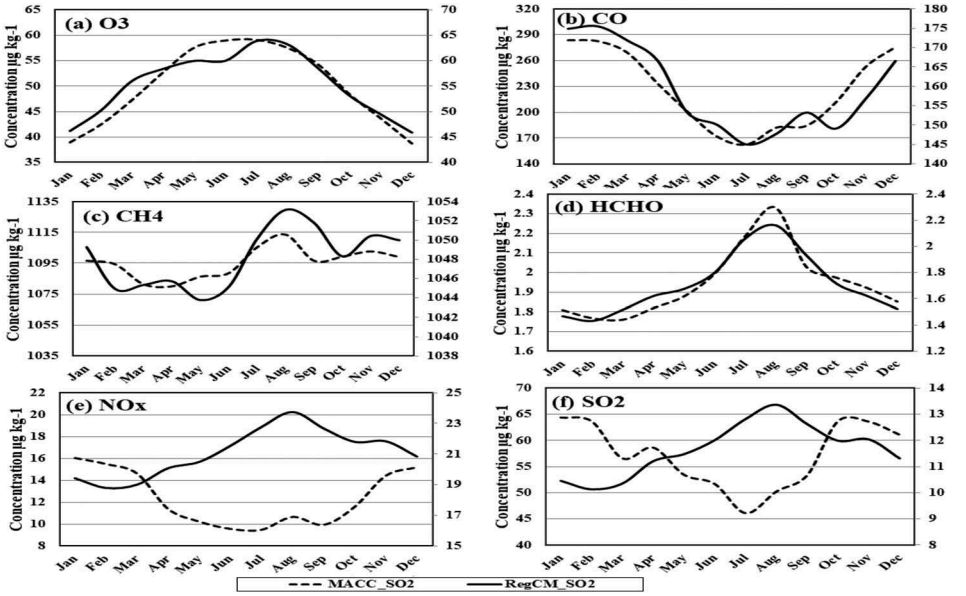

Figure 3. Annual cycle of MACC, (dashed line lift axis) and RegCM4-CHEM, (solid line right axis): (a) O_3, (b) CO, (c) CH_4, (d) HCHO, (e) NOx and (f) SO_2 near-surface area average during 2003–2010.

there is a good agreement between the behaviour of the monthly mean values of observed and simulated CH_4 concentrations, and the simulated CH_4 concentrations are underestimating the observed for all months. The simulated monthly values of CH_4 ranged between 1053 and 1044 µg/kg, while the observed values of CH_4 ranged between 1079 and 1038 µg/kg. The time series of monthly mean values of the simulated HCHO concentrations have the same behaviour of the corresponding observed, where the higher values occur during the months of July, August, and September while the lower values appear during the winter months (Figure 3(d)). Generally, the simulated HCHO concentrations are underestimating the observed throughout all months of the year. An obvious disagreement between the behaviour of the time series of monthly mean values of the observed and simulated NO_x and SO_2 for all months of the year (Figure 3(e,f)), where the inverse relationship between the observed and simulated NO_x and SO_2 appears. A discrepancy between the simulation and observation is that the relationship between NO_x and SO_2 is stronger in the simulation than in observation.

It is clear that the higher correlation between observed and simulated atmospheric variables occurs with temperature (0.98) and relative humidity (0.61), the higher correlation between observed and simulated pollution variables occurs with O_3 (0.75) and CO (0.55). Also, it is obvious that values of the normalised standard deviation for the observed and simulated atmospheric variables are nearly equal, while a large difference occurs between the normalised standard deviation for the observed and simulated pollution variables. The values of the normalised standard deviation for the observed pollutants variables are very greater than those of the simulated pollution variables. Generally, it can be saying that RegCM4 reduces the variability in the values of pollutants variables.

3.3. RegCM4-CHEM and MACC vertical cross-section

Figure 4 shows the area average of the monthly height variation for the observed (MACC) and simulated (RegCM4-CHEM) meteorological variables T, RH, u and v component. The comparison between the observed and simulated temperature illustrates that there is a good agreement between the behaviour of *T* for all months and at all levels (Figure 4(a,b)). Figure 4(c,d) illustrate the area average of the monthly height variation for the observed and simulated RH, generally, a good agreement occurs between the observed and simulated RH above 500 hPa. Three different differences appear, the first one, higher values of RH (MACC) lies between 1000 and 700 hPa especially in the winter and autumn seasons, while in RH (RegCM4-CHEM) the higher values 850–500 hPa in the winter and autumn seasons. The lowest values of RH occur between 700 and 200 hPa during the months from May to September. The higher values of the zonal wind occur in associated with the subtropical jet between 400 and 100 hPa especially at 200 hPa during the winter, spring and autumn months (Figure 4(e,f)). The higher values of the meridional wind occur also between 400 and 100 hPa especially at 200 hPa during the period from May to October (Figure 4(g,h)). The only small difference in the observed and simulated meridional wind occur above 500 hPa for the winter and spring months.

Figure 5 shows the area average of the monthly height variation for the observed (MACC) and simulated

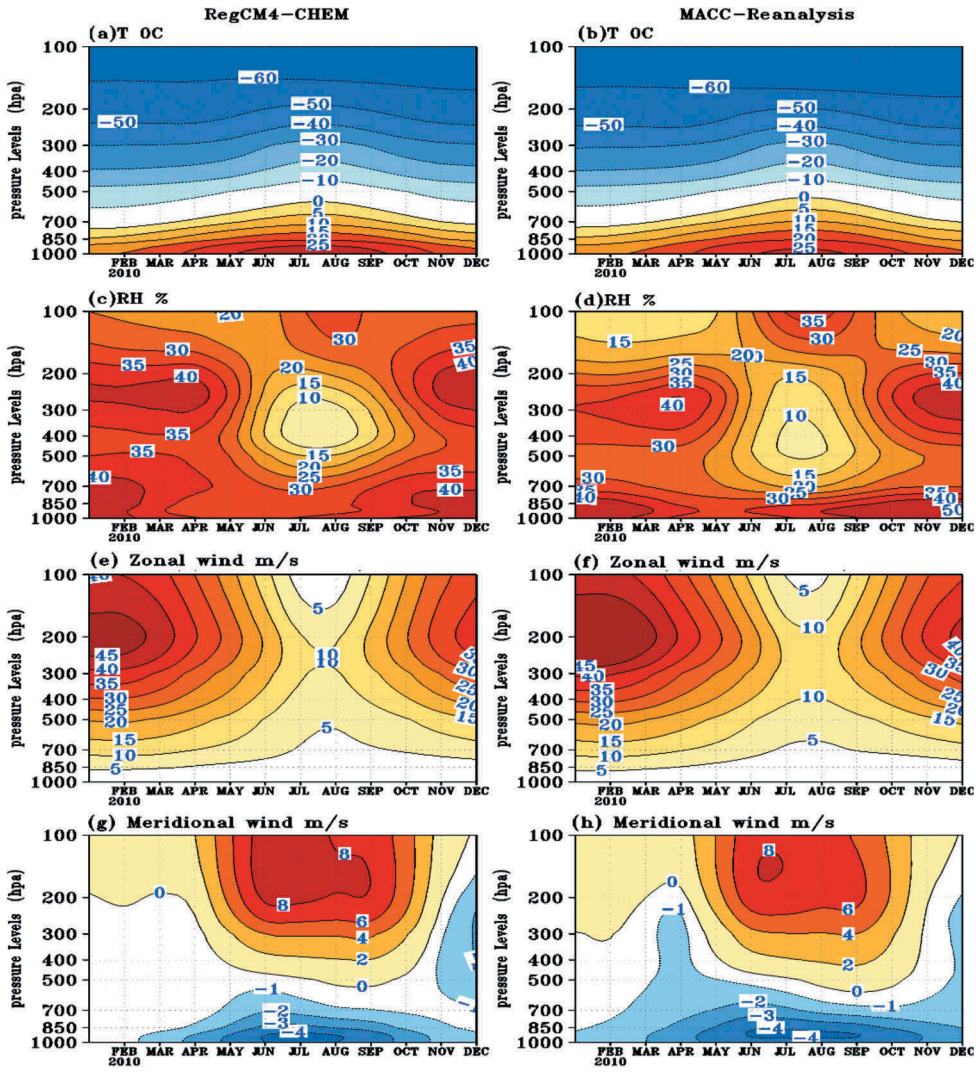

Figure 4. The annual cycle of RegCM4-CHEMand MACC (2003–2010): *T*, RH, zonal wind and meridional wind near-surface area average during 2003–2010.

(RegCM4-CHEM) pollution variables O_3, CO, CH_4, HCHO, NO_x and SO2. Generally, the values of O_3 increase from surface to the higher levels (Figure 5(a, b)). Their values increase during the spring and summer months with a maximum in July and August. The patterns of monthly mean-height variation of observed and simulated O_3 are very similar. The simulated values of O_3 are greater than those corresponding in observed O_3, the difference in the lower and middle layer (1000–400 hPa) reaches 20 μg/kg, while in the upper layer is greater than 50 μg/kg. Figure 5(c,d) show that the pattern of the area average of the monthly height variation of simulated CO is different from observed (MACC) CO. The values of observed CO are greater than of the simulated CO near the surface (below 850 hPa). Above 850 hPa the values of observed CO decrease gradually with height, it reaches to lower than 50 μg/kg at 100 hPa during the months of winter, spring and autumn. The vertical distribution of simulated CO in summer months is different from observed CO, where there are lower values between 850 and 200 hPa, these values ranged between 80 and 90 μg/Kg. Figure 5(e,f) illustrates that the values of simulated and observed CH_4 are equal in the lower layer (at the surface). Above 850 hPa the values of simulated CH_4 decrease gradually with height, it reaches to lower than 950 μg/kg at 100 hPa during the months of winter and spring. The vertical distribution of the observed values of CH_4 is nearly equal to the simulated, while the pattern of the simulated and observed of CH_4 is different. Figure 5 (g,h) show a good agreement between the observed and simulated vertical distribution values of HCHO. The maximum concentration of HCHO appears at the lower layer, its values decrease gradually with height, the large values occur in the summer months above 900 hPa. The patterns of monthly mean- height variation of observed and simulated NO_x are similar, generally the values of NO_x concentrated below 925 hPa level (Figure 5 (i,j)). The simulated values of NO_x are greater than those corresponding in observed NO_x at the surface; the greatest difference appears in the summer months. Although there are great differences between the simulated and observed SO_2 values, the highest concentration is found

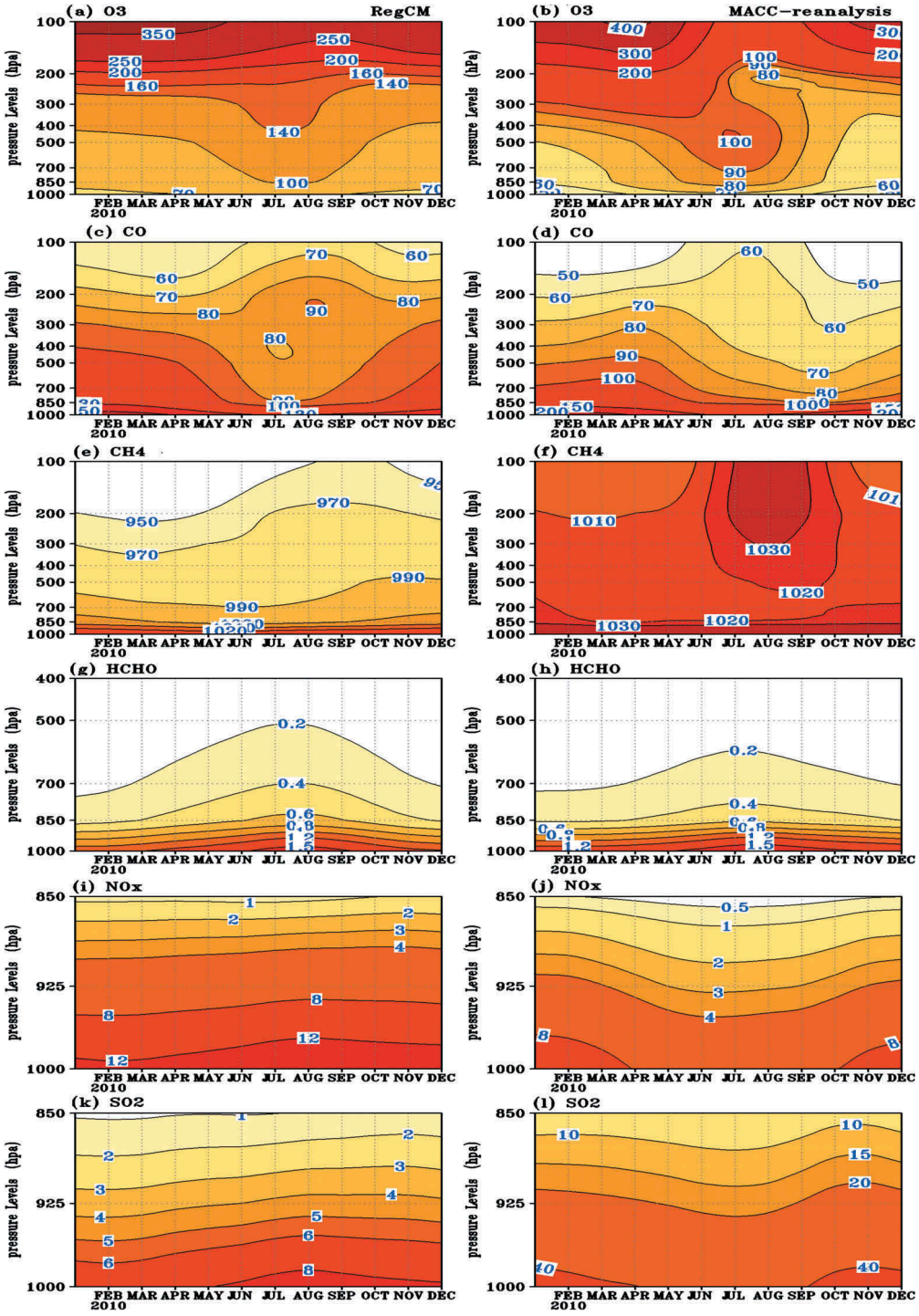

Figure 5. The annual cycle of RegCM4-CHEMand MACC: O_3, CO, CH_4 HCHO, NOx and SO_2 near-surface area average during 2003–2010.

in the lower levels and gradually decreases with the height from both datasets (Figure 5(k,l)).

3.4. Characteristics of the simulated pollutants

3.4.1. Seasonal patterns of atmospheric variables

The atmospheric variables (pressure, temperature, relative humidity and wind) have a significant impact on increasing and decreasing pollutants concentration and emission (Zeng and Zhang 2017). The wind plays an important role in transporting pollutants in different regions around the world, and varies in speed and direction from one season to another (Shalaby et al. 2012; Ojumu et al. 2013).

Figure 6 shows the horizontal distribution of the seasonal and annual average values of relative humidity, temperature and wind speed, and direction at 1000 hPa. In winter the dominant pressure systems affecting the weather of Egypt are the Siberian high, the Subtropical high, the Red Sea Trough (the northward extension of Sudan monsoon low) and the travelling midlatitude cyclones. The wind is generally westerly over the

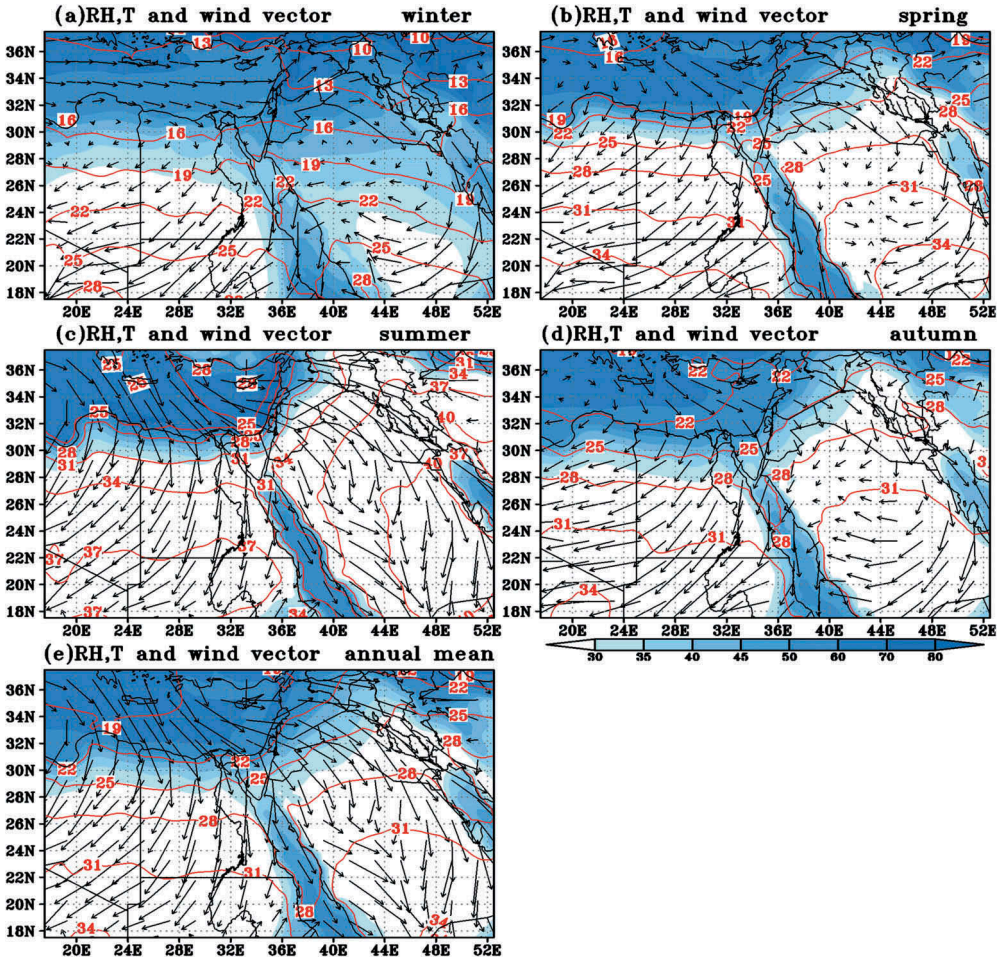

Figure 6. RH (shaded), temperature (contour) and wind vector seasonal and 10 year's average.

Mediterranean Sea, northwesterly over the north of Egypt and northerly to northeasterly over east Egypt (Figure 6(a)). Meanwhile, the relative humidity has the largest values over the Mediterranean Sea and north Egypt (exceeds 80%) and temperature increases from north to south with ranges from 10 to 25°C (Figure 6 (a)). In spring the dominant pressure systems are nearly the same as in winter but the Siberian high shifted northeastward and the Red Sea trough oscillates northward to cover the east of Mediterranean (Figure 6(b)). The wind speed increases relatively and does not change in direction compared to the winter season except it changes to northwesterly in the middle and south of Egypt. Regarding relative humidity, it is relatively smaller than winter and decreases from north to south (80–150%), while the temperature is greater than winter and increases from the north (20°C) to the south (35°C) (Figure 6(b)). In summer the two dominant pressure systems are the subtropical high and Indian monsoon low when subtropical high prevails and extended easterly, the Indian monsoon is retarded eastward and vice versa (Figure 6(c)). The wind speed increases than in the other seasons and its direction become northerly over Egypt, whereas the relative humidity decreases and ranges from 50% over the north to 15% over the south of Egypt and the highest temperature are recorded in this season (25–40°C) as compared to other seasons (Figure 6 (c)). In autumn the dominant pressure systems, wind speed and direction, relative humidity, and temperature patterns are nearly the same as in spring (Figure 6(d)). Finally, the annual distribution of wind illustrates that the dominant wind north of 30° N is westerly; it changes to northwesterly over the middle and south of Egypt (Figure 6(e)). Moreover, the relative humidity increases gradually northward to reach its higher values north of 30° N and over the Red Sea. Also, the temperature pattern has a reverse pattern compared to the relative humidity, where it decreases gradually from the south (~35°C) to the north (~20°C) of Egypt (Figure 6(f)).

3.4.2. Seasonal patterns of pollutants

The surface O_3 production and destruction controlled by dynamical and photochemical factors (e.g. wind and temperature), where the wind (westerly, northerly and northwesterly) transport the pollutants O_3 from the European region to Egypt (Shalaby et al. 2012). Moreover, surface O_3 concentration is mainly affected by some of the other pollutants (VOCs, NO_x and NO_y) concentration (Vautard et al. 2005; Steiner et al. 2014). Figure 7 shows the horizontal distribution of the simulated O_3, CO, HCHO, VOCs and NO_y seasonal mean (2001–2010) for surface O_3 concentration, while Figure 8

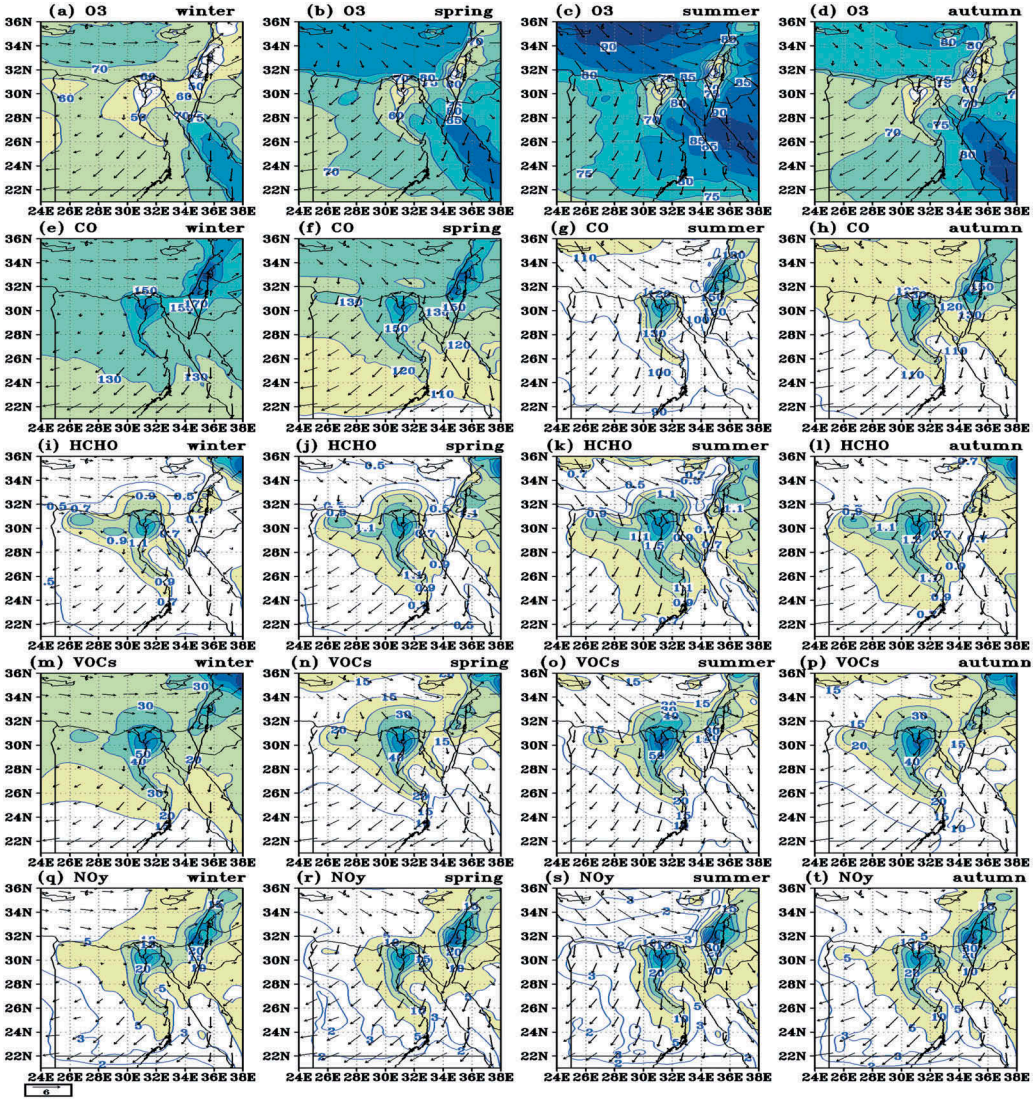

Figure 7. RegCM4-CHEM simulated seasonal mean (2001–2010) for surface O_3, CO, HCHO, VOCs and NO_y mixing ratio.

illustrates their annual mean. It is clear the higher values of surface O_3 occur in summer (Figure 7(c)) while the lower values occur in winter (Figure 7(a)). The values of O_3 are relatively moderate and similar in both spring and autumn (Figure 7(b,d)). In general, the higher surface O_3 over the Mediterranean and the Red Sea has been found during the seasonal and annual mean (Figures 7(a–d) and Figure 8(a)) with a range of 75–90 (μg/kg), whereas the lower values are found over the study area and the eastern Mediterranean with a range of 54–57 (μg/kg). The higher values of O_3 are attributed to the wind transfer from Europe and other regions, and the lower values are attributed to urbanisation which in turn leads to high levels of VOC, NO_x and NO_y.

CO is a primary pollutant and emitted from fuel combustion and agriculture activities as the main source. The CO concentration has been governed by several processes such as emissions, transport, photochemical reactions, deposition (dry and wet deposition) and atmospheric conditions. CO beings the main sink for OH (due to its reaction with OH) and hence affects the oxidising capacity of the troposphere by modulating the concentration of various atmospheric species (Park et al. 2009; Lelieveld et al. 2016; Zeba et al. 2019). Figure 7 (e–h) shows the horizontal distribution of the simulated seasonal and annual mean (2001–2010) for surface CO concentration. Figure 7(e) illustrates that the higher values of CO (130–210 μg/kg) appear in winter due to the increase in fuel combustion. The second higher values occur in spring, it ranges between 110 and 200 μg/kg (Figure 7(f)). The values of CO during the autumn and the summer ranges between 100 and 190, and 90 and 160 μg/kg respectively (Figure 7(g,h)), while the mean annual values of CO range between 110 and 200 μg/kg (Figure 8(b)). It is clear that CO decreases gradually from north of Egypt (south Europe and the Mediterranean) to the south followed the wind direction during all seasons with high values over the study area and Eastern Mediterranean (160–210 μg/kg) affected by increased population and high transportation density. As a result of CO lifetime which extends from several days to several weeks (WMO 1995; IPCC 2007; EPA 2010),

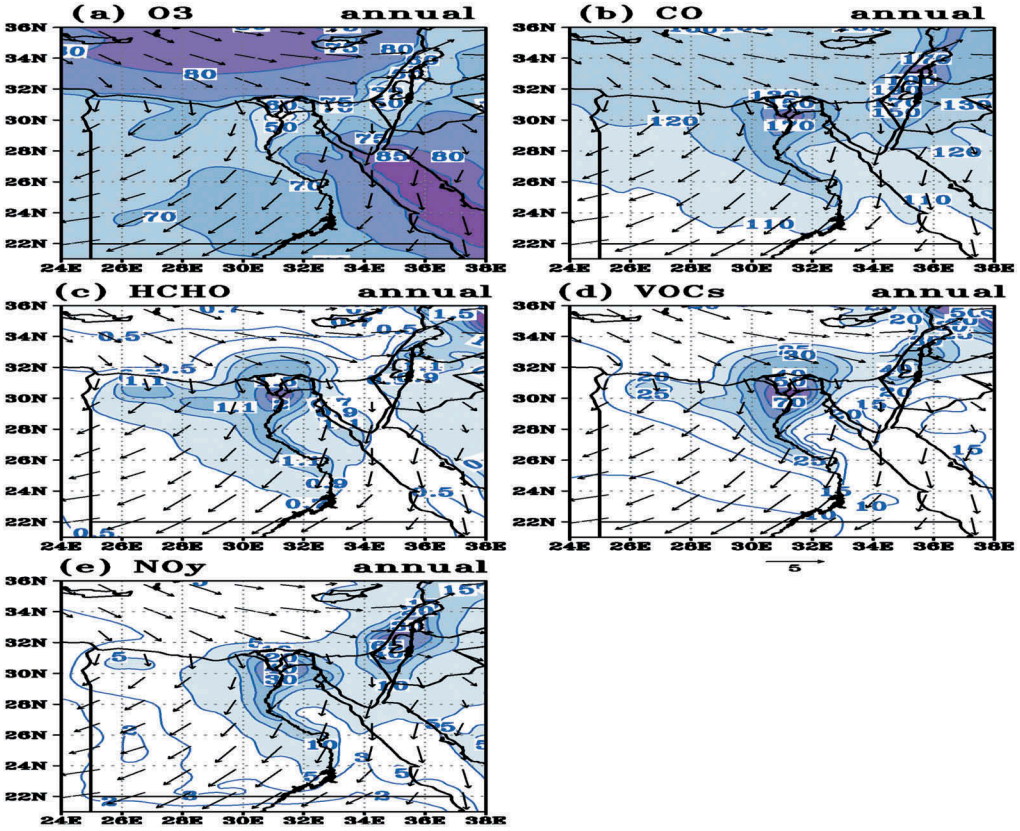

Figure 8. RegCM4-CHEM simulated annual mean (2001–2010) for surface O_3, CO, HCHO, VOCs and NO_y mixing ratio.

their maximum values in winter continue up to the spring. The lowest values of CO in summer are due to the fuel combustion is decreasing, while it begins to increase with the onset of autumn due to the harvest, biomass burning and increased fuel combustion in late autumn.

HCHO is a primary pollutant and considered as an intermediate gas in the hydrocarbon compounds oxidation and it is a species of VOC group. The lifetime of HCHO is short (several hours), and its reaction with OH and photolysis reactions are an important source of CO. Because of its high activity and short lifetime of HCHO, it spreads by the wind for relatively short distances around the source compared to O_3 and CO. Figure 7(i-l) and Figure 8(c) shows the horizontal distribution of the simulated seasonal and annual mean (2001–2010) for surface HCHO concentration respectively. The values of HCHO ranges between 0.6 and 2.7 μg/kg in summer, 0.6 and 2.4 μg/kg in autumn, 0.6 and 2.2 μg/kg in spring, 0.6 and 2.0 μg/kg in winter and 0.6 and 2.4 μg/kg as annual mean. Thus, the higher values of HCHO occur in summer while the lowest values found in winter, high temperature and an abundance of OH are the main reasons for increasing HCHO during summer, the inverse is true in winter.

The most important pollutant is VOCs; it is emitted into the troposphere from anthropogenic and biogenic sources (Placet et al. 2000). Previous studies have exposed that the VOCs are a chief species in the atmospheric oxidation reactions. CO, NO_x, NO_y SO_2 and VOCs caused a long series of chemical and photochemical interactions in the presence of OH, which effects on the ozone concentrations in urban areas, regional and global troposphere (Logan 1985), acid deposition and secondary pollutants construction over gas and particle interaction for NO_x, VOCs and SO_2 compounds (Sillman et al. 1995). Other studies show that NO_x-sensitive conditions are usually related with small values of NO_y (concurrent with the time of elevated O_3) and those VOCs-sensitive conditions are linked with greater NO_y (Milford et al. 1994; Sillman and He 2002; Beekmann and Vautard 2010). The NO_y threshold for VOC as opposed to NO_x sensitivity can contrast depending on the site, with interregional differences caused by the overall VOC/NO_x ratio, meteorological conditions and the influence of ozone advection. VOCs are significant compounds in atmospheric reactions, because they regarded as the major precursors of secondary organic aerosols and secondary pollutants in photochemical reactions. The presence of HCHO is related to the release of VOCs by biomass and fuel burning. The higher values of VOCs occur in winter due to the high fuel combustion and it ranges between 15 and 90 μg/kg (Figure 7(m)), while the lower values occur in summer and it range between 10 and 70 μg/kg (Figure 7(o)). The values of VOCs during spring, autumn (Figure 7(n) and (p)) and annual mean (Figure 8(d)) are nearly similar and ranges

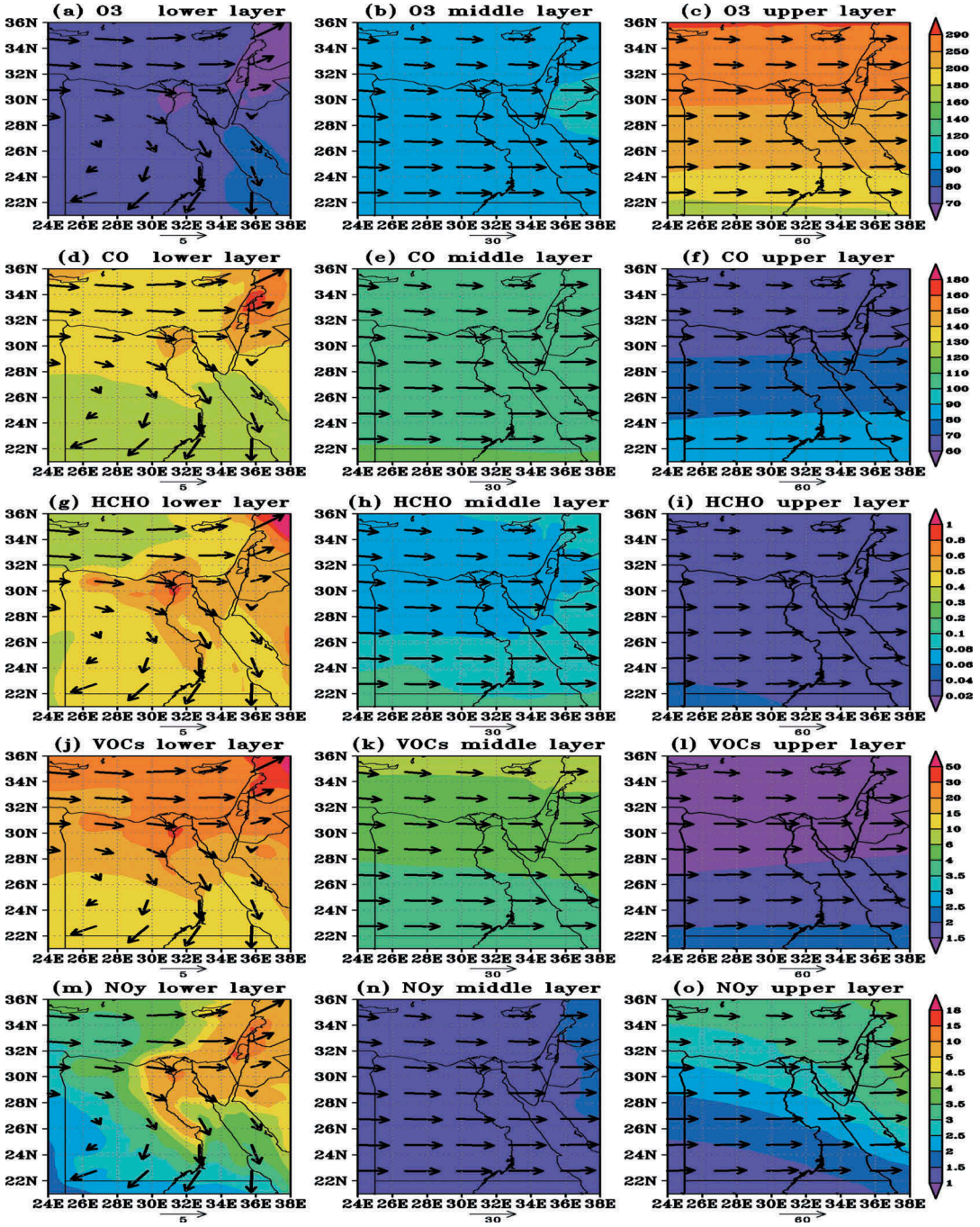

Figure 9. The annual average of the simulated pollutants concentration over 10 years (2001–2010); the above first row for O_3, second row for CO, third row for HCHO, fourth row for VOCs and fifth row for NO_y; the left, middle and right columns represent lower (1000–850 hPa), middle (700–300 hPa) and upper (250–100 hPa) layers respectively.

between are 10 and 80 μg/kg. The study area is covered mostly by high VOCs values, where the ranges in all seasons and annual mean are 30–70 μg/kg, these high values of VOCs are attributed to the high population and greatest activities in this area.

Thus, the high concentration of NO_y is usually located near the main sources of NO_x. The ratio between NO_y and NO_x has an important role in atmospheric reactions especially during the loss and production of O_3 (Shalaby et al. 2012). NO_y and some other primary pollutants in the presence of OH produce a long series of atmospheric reactions that affect O_3 concentration in urban areas, secondary pollutants construction and acid deposition (Sillman et al. 1995). NO_y has two significant concentration spots located over the study area and Eastern Mediterranean with values exceed 60 μg/kg, while the highest NO_y values over the rest of the selected area reach 25 μg/kg. NO_y concentration over the selected area has large values during summer and autumn ranged from 10 to 65 μg/kg (Figure 7(s,t)). The lowest NO_y concentrations occur in winter with range 5–55 μg/kg (Figure 7(q)) followed by spring (Figure 7(r)) with range 5–60 μg/kg which is similar to the annual mean (Figure 8(e)). The

highest NO_y concentrations that detected over the two spots are significantly correlated with human activates (vehicle motor, power generation stations, oil refineries and agricultural practices).

From the previous results, it is obvious that the simulated pollutants (O_3, CO, HCHO, VOCs and NO_y) concentrations and their seasonal spatial distributions are significantly influenced directly and indirectly by atmospheric conditions (temperature, relative humidity and wind) and urbanisation. The simulated O_3 concentration is highly sensitive to temperature, other studied pollutants, as increasing these factors coincides with the decrease and removal of O_3; these findings are agreeing with the results documented by Velchev et al. (2011) and Shalaby et al. (2012). Population increase and urbanisation in the study area led to a decrease in O_3 concentrations, especially in polluted and hazy regions, with increased CO, NO_y, NO_x and VOCs, which match the results from Sillman et al. (1995). The westerly and northwesterly winds increase the concentration of the pollutants over the study area due to their transport from the European region across the Mediterranean Sea and other regions as presented by Steiner et al. (2014).

3.5. Pollutants vertical analysis

3.5.1. The annual mean of pollutants on the different layers

The simulated annual average of O_3, CO, HCHO, VOC and NO_y concentration over 10 years (2001–2010) have been divided vertically into three different atmospheric layers. The lower layer (1000–850 hPa) represents the average of 1000, 925 and 850 pressure levels, while the middle layer (700–300 hPa) denotes the average of 700, 500, 400 and 300 pressure levels and finally, the average of 250, 200, 150 and 100 pressure levels is considered as the upper layer. The horizontal spatial distribution over Egypt for the simulated pollutants (rows) on each layer (columns) is shown in Figure 9.

It is clear that the concentration O_3 increases gradually from the lower layer to the upper layer due to its proximity to its main source in the stratosphere, where its values on the lower layer ranged between 60 and 90 μg/kg and in the middle layer between 90 and 100 μg/kg while in the upper layer 170 and 300 μg/kg (Figure 9(a–c)). It is obvious that O_3 is transported from the upper layer to middle and then to the lower layer leading to increasing the surface O_3 as illustrated in Figure 5(a). Most of the selected area in the lower layer is covered by O_3 concentration less than 80 μg/kg except over the study area, which has the lowest values (less than 70 μg/kg) due to the increasing other pollutants and Red sea which has the largest values (80–90 μg/kg) due to wind transporting. The middle layer is often having a homogenous distribution of O_3 concentration (about 95 μg/kg), while the upper layer has an O_3 concentration range of 200–290 μg/kg over the most area except south of 24° N has O_3 concentration less than 200 μg/kg.

In contrast to O_3, the other pollutants CO, HCHO, VOCs and NO_y have the largest concentrations in the lower layer (the nearest layer to the surface) which is considered the main emission pollutant source due to human activities. The lowest concentrations of these pollutants are detected on the upper layer except for NO_y in the middle layer. The concentrations of CO in the lower layer ranged from 120 to 180 μg/kg with values greater than 150 μg/kg over the study area, where it is greater than 140 μg/kg north of 30° N and less than 140 μg/kg south of 30° N (Figure 9(d)). While CO concentrations in the middle layer (Figure 9(e)) reached to 115 μg/kg and most of the upper layer (Figure 9(f)) is covered by values less than 90 μg/kg, where its concentrations have a semi homogeneous distribution in the middle and upper layers. The largest concentration of CO is found in the northern part of the selected area due to northwesterly flow that transports CO from the European region. The HCHO concentrations distribution in the lower, middle and upper layer is shown in Figure 9(g), (h) and (i) respectively. The maximum HCHO concentration is noticed in the lower layer (0.15–1 μg/kg) with the largest values over the study area, Nile valley and eastern Mediterranean (0.5–1 μg/kg). While it decreases gradually with height with values of 0.05–0.15 μg/kg in the middle layer and values of 0.02–0.05 μg/kg (seems to be not present) in the upper layer. In the middle layer, the largest concentration of HCHO is found south of 25° N (0.09–0.15 μg/kg) and the smallest is noted north of 25° N (0.05–0.09 μg/kg) as shown in Figure 9(h). In the upper layer, most of the selected area south of 32° N has homogenous HCHO concentration values less than 0.04 μg/kg, as seen in Figure 9 (i). The VOCs concentrations in the lower layer (Figure 9(j)) are highest in the study area and the northeastern corner of the selected area with values exceeds 30 μg/kg. The dominant values north of 30° N are 20–30 μg/kg and south of 30° N are 10–20 μg/kg. In the middle layer (Figure 9(k)) VOCs concentration ranges from 2.5 to 10 μg/kg around 32° N, while in the upper layer (Figure 9(l)) it has an increasing gradient from north to south with values between 1 and 2.5 μg/kg. The NO_y concentration has two largest hotspot areas over the study area and the eastern Mediterranean with values ranges from 10 to 15 μg/kg in the lower layer (Figure 9(m)). Also the Nile valley, Sinai and most of the eastern Mediterranean region have nearly 5–10 μg/kg NO_y concentration. The NO_y concentration in the middle layer (Figure 9(n)) is homogeneous and has values around 1 μg/kg. Finally, the NO_y concentration in the upper layer (Figure 9(o)) is generally greater than in the middle layer because NO_y contains NO_x which regarded as a catalyst in O_3

loss and production. In addition, the NO_y concentration increases gradually in the upper layer from southwest to northeast of the selected area with values between 1.5 and 5 μg/kg.

3.5.2. Total column mixing ratio

The area average of annual cycle total column (from 1000 to 100 hPa) over the study area for the simulated pollutants (O_3, CO, HCHO, VOCs and NO_y) are illustrated in Figure 10. The total column annual cycle of pollutants depends on temperature, geography, location and prevailing synoptic situation (Sillman et al. 1995; Roelofs et al. 2005; Stevenson et al. 2005).

Figure 10(a) shows the monthly area average (study area) of the total column of the O_3 amount for the period of study. It is clear that the higher values of O_3 occur during the period from January to August with two maximums in May and July (1710 μg/kg). The lower values of O_3 occur in autumn months and December with the lowest one in October (1470 μg/kg). Figure 10(b) shows the monthly area average (study area) of the total column of CO amount for the study period. The higher values of CO appear in winter months, March and April with a maximum value in January (1130 μg/kg), these higher values attributed to the highest human activates during these months. The lower values of CO appear in May, summer months and October with a minimum value at July (935 μg/kg), it is attributed to starting gross biomass burning during autumn (Steiner et al. 2014). Figure 10(c) shows the monthly area average (study area) of the total column of the HCHO amount for the study period. The higher values of HCHO occur in summer months and September with a maximum value in August (4.6 μg/kg). The lower values of HCHO appear in winter months and March with a minimum value in February (2.7 μg/kg). The HCHO concentration is sensitive to temperature, NOx and VOCs in the presence of the OH radical. Figure 10(d) shows the monthly area average (study area) of the total column of VOCs amount for the study period. It is obvious that VOCs have two peaks and the higher values of VOCs occur in winter months, July and August with two maximum values in January and August (113 and 1114.6 μg/kg). The lower values of VOCs appear in spring and autumn months with a minimum value in April (91 μg/kg). The higher values of VOCs in summer attribute to the high concentration of OH radicals which considered the main factor in the VOCs loss and production. Figure 10(e) shows the monthly area average (study area) of the total column of NO_y amount for the study period. It is clear that the higher values of NO_y occur during the summer months and September with a maximum in August (59.5 μg/kg). The lower values of NO_y occur in winter with the lowest one in January (21.9 μg/kg).

Various studies that used the RegCM4-CHEM illustrate that the NO_x maximum concentration occurs in winter, while the minimum values occur in the summer;

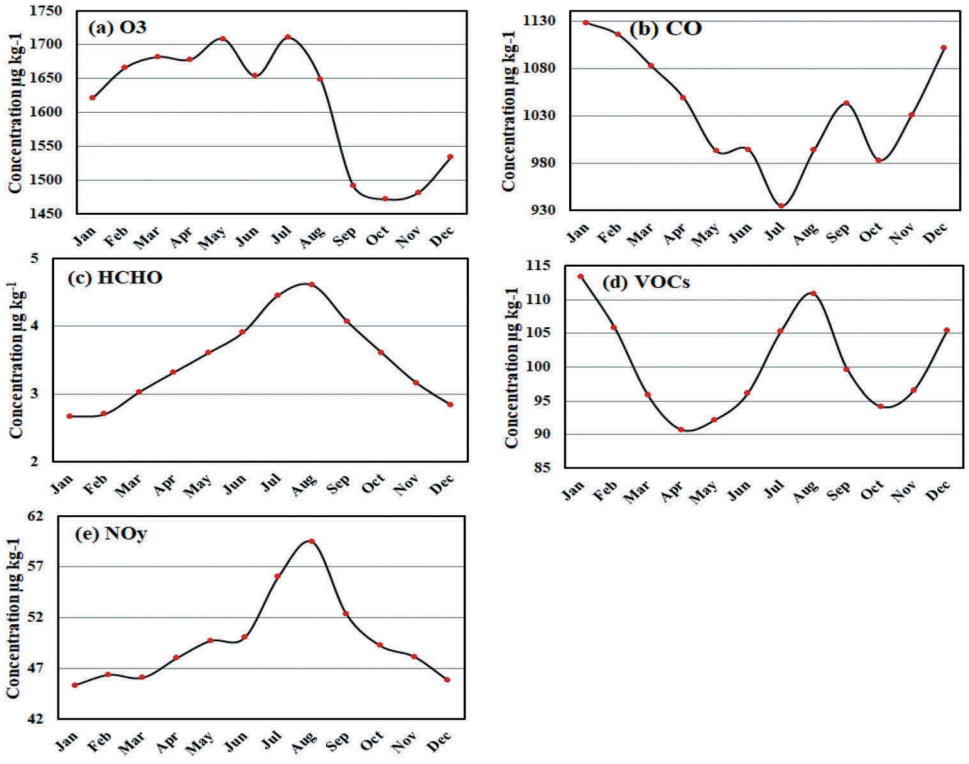

Figure 10. Area average of annual cycle total column (1000–100 hPa) over the study area for O3, CO, HCHO, VOC and NOy.

but another study indicate that the NO_x maximum concentration values occur in the summer and minimum occur in the winter (Shalaby et al. 2012; Steiner et al. 2014; Mostafa et al. 2018).

3.5.3. Monthly-height cross-section of pollutants anomalies

The variation in the annual cycle of pollutants concentrations with height is very sensitive to seasons. Figure 11 illustrates the anomaly of the monthly mean from the annual mean of our pollutants at each pressure level for all months of the year. It is obvious that O3 has a positive anomaly during the period from May to September in a layer between 1000 and 200 hPa with higher values in the summer season especially between 600 and 300 hPa. Also, there is another positive anomaly appears during the months of winter and spring above 300 hPa level with maximum values above 150 hPa (Figure 11(a)). However, O3 has negative anomalies at the months of winter and spring between 1000 and 300 hPa and at all levels during the autumn months, the higher negative anomaly occurs in the summer above 200 hPa with a maximum above 150 hPa. The negative anomalies of O_3 below 300 hPa during autumn, winter and spring are weak where it ranges between 9 and 20 μg/kg. Figure 11(b) shows the anomaly of the monthly mean from the annual mean of CO. The figure illustrates that CO has a positive anomaly from the surface to 300 hPa during the winter and spring months with maximum values between 1000 and 700 hPa at January, February, and March, the maximum values are greater than 20 μg/kg at February below 900 hPa. The second positive anomalies of CO occur in June to October above 300 hPa with higher values in August and September between 400 and 250 hPa (> 20 μg/kg). CO also has two periods of negative anomalies, the first during the winter and spring months above 250 hPa with maximum values in April and May between 200 and 150 hPa. The second period of negative anomalies occurs between May and November from 1000 to 300 hPa, with a maximum between June to September from surface up to 400 hPa.

Figure 11(c) shows the anomaly of HCHO, it illustrates that the higher negative anomaly occurs in November, winter months and March with maximum

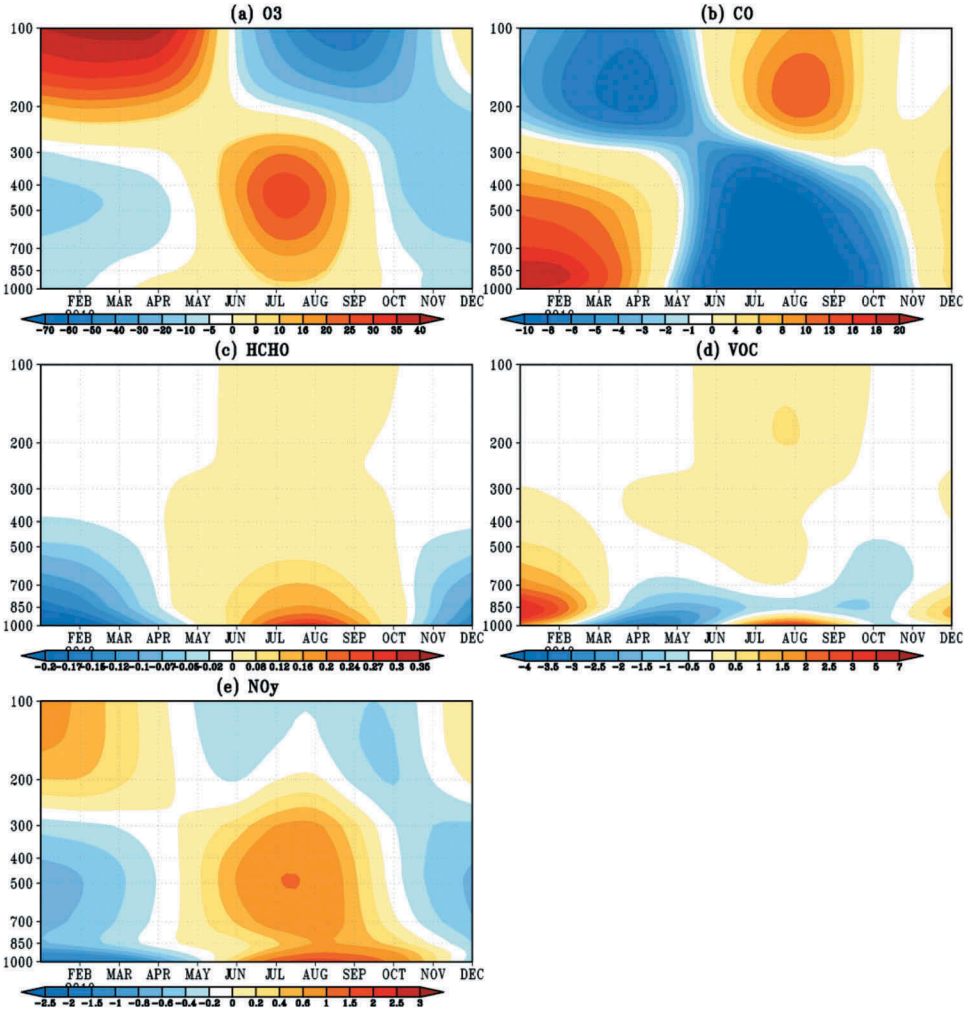

Figure 11. The annual cycle height anomalies of the simulated O_3, CO, HCHO, VOC and NO_y 10-years area average mass concentrations over Egypt.

values below 600 hPa in winter months. The figure also illustrates that the positive anomaly occurs in the period from May to October with Maximum positive anomaly below 700 hPa in July and August. Also, it can be noticed that there are lower values of positive anomalies extended from 600 to 100 hPa. Figure 11(d) shows the VOCs anomalies, where the positive anomalies occur in July, August and September at 1000 hPa and in December, January and February around 900 hPa, while during March, April, May, Jun, October and November the VOCs has a negative anomaly. Finally the NO_y anomaly is shown in Figure 11(e), where it has a positive anomaly in August during summer below 200 hPa and in February during winter above 200 hPa. Meanwhile, it has a negative anomaly during autumn above 700 hPa and during winter below 300 hPa.

Table 1 shows the seasonal and annual mean of O3, CO, HCHO, VOCs and NO_y net flux over the study area. All pollutants have a negative flux over the study area this means that the incoming pollutants are greater than the outgoing pollutants that are that study area is a sink for all the pollutants during all seasons. The negative flux means the accumulation of pollutants over ND. The highest values of flux matching to the highest northerly wind in summer that indicates the movement of the pollutants from European regions to ND. The lower values of flux occur in winter due to the wind it's weaker.

4. Conclusion

In this work we use the RegCM4-CHEM model to study the characteristics of some simulated pollutants (O_3, CO, HCHO, VOCs and NO_y) over Egypt during the period 2001–2010. A good agreement has been found when comparing the model results with ERA-int for meteorological parameters and MACC-reanalysis for pollutants parameters, which indicate the ability of the model in simulating the meteorological and pollutants parameters. The most significant findings from the analysis of the characteristics of our interesting simulated pollutants (O_3, CO, HCHO, VOCs and NO_y) are as following:

(1) The higher surface O_3 has been found over the Mediterranean and Red Sea during the seasonal and annual mean, while the lower values are found over the study area and the eastern Mediterranean. These higher values of O_3 are attributed to the wind transfer from Europe, and the lower values are attributed to urbanisation which in turn leads to high levels of VOC, NO_x and NO_y. The concentration O_3 increases gradually from the lower layer to the upper layer due to its proximity to its main source in the stratosphere. Also, it is found that O_3 has higher values (positive anomaly) during the period from May to September that indicates their sensitivity to temperature and sinking air above the dominant subtropical high pressure during these hot months.
(2) The concentration of CO decreases gradually from north of Egypt (south Europe and the Mediterranean) to the south followed the wind direction during all seasons with high values over the study area and Palestine affected by increased population and high transportation density. Higher values of CO occur in winter and slightly less in spring (positive anomaly) associated with the largest amounts of fuel burning in winter. The lowest values of CO appear in summer due to the fuel combustion is decreasing, it begins to increase with the onset of autumn due to the harvest, biomass burning and increased fuel combustion in late autumn. The maximum concentration of CO is found in the northern part of the selected area due to northwesterly flow that transports CO from the European region.
(3) The higher values of HCHO (over our study area) occur in summer associated with high temperatures and an abundance of OH, while its lowest values appear in winter. The maximum HCHO concentration is noticed in the lower layer, while it decreases fustily with height. A higher negative anomaly of HCHO appears in November, winter months and March, where the positive anomaly occur in the period from May to October
(4) The VOCs are significant compounds in atmospheric reactions, because they regarded as the major precursors of secondary organic aerosols and secondary pollutants in photochemical reactions. The presence of HCHO is related to the release of VOCs by biomass and fuel burning. The study area is covered mostly by high VOCs values, these high values of VOCs are attributed to the high population and greatest activities in this area. The highest VOCs concentrations occur in the lower layer while it decreases gradually with height.
(5) The highest values of NO_y concentrations detected over the ND area that is significantly correlated with human activate (vehicle motor, power generation stations and agricultural practices). The lower values of NO_y occur in winter months below 300 hPa with a maximum

Table 1. The near-surface net flux of pollutants (O_3, CO, HCHO, VOCs and NO_y) over ND.

Pollutant	Winter	Spring	Summer	Autumn	Annual
O3	−9.99333	−328.217	−476.3	−421.51	−309.005
CO	−39.6667	−771.243	−962.207	−1010.99	−696.026
HCHO	−0.27	−6.72	−10.5067	−10.18	−6.91917
VOCs	−7.26	−195.58	−283.723	−302.303	−197.217
NOy	−3.76	−71.79	−104.067	−106.053	−71.4175

at the surface, while the higher values appear in summer months, September and October in the layer between 1000 and 300 hPa. The concentration of NO_y in the upper layer is generally greater than in the middle layer because NO_y contains NO_x which regarded as a catalyst in O_3 loss and production.

(6) Generally, it is found that the simulated pollutants (O_3, CO, HCHO, VOCs and NO_y) concentrations and their seasonal spatial distributions are significantly influenced directly and indirectly by atmospheric conditions (temperature, relative humidity, and wind) and urbanisation. The westerly and northwesterly winds increase the pollutants concentrations over the study area due to their transportation from the European region across the Mediterranean Sea as presented by Steiner et al. (2014).

(7) The concentration of the simulated O_3 is highly sensitive to temperature and other studied pollutants, where the increase of these factors coincides with decrease and removal of O_3; these findings are agreeing the results documented by Velchev et al. (2011) and Shalaby et al. (2012). Also, population increase and urbanisation in the study area led to a decrease in O_3 concentrations, especially in polluted and hazy regions, with increased CO, NO_y, NO_X and VOCs, which match the results from Sillman et al. (1995).

(8) In contrast to O_3, the other pollutants CO, HCHO, VOCs and NO_y have the largest concentrations in the lower layer (the nearest layer to the surface) which is considered the main emission pollutant source due to human activities. The lowest concentrations of these pollutants are detected on the upper layer except for NO_y in the middle layer.

Disclosure statement

No potential conflict of interest was reported by the authors.

ORCID

Mostafa Morsy http://orcid.org/0000-0002-0271-2074

References

Abdul-Wahab SA, Bouhamra WS. 2004. Diurnal variations of air pollution from motor vehicles in residential area. Int J Environ Stud. 61(1):73–98. doi:10.1080/00207230320001300 34Aboel.

Beekmann M, Vautard R. 2010. A modelling study of photochemical regimes over Europe: robustness and variability. Atmos Chem Phys. 10:10067–10084. doi:10.5194/acp-10-10067-2010.

CAPMAS (Central Agency for Public Mobilization and Statistics). 2017. Statistical yearbook 2017. Egypt: Arab Republic of Egypt. pp. 665.

Dickinson RE, Hauglustaine D, Heinze C, Holland E, Jacob D, Lohmann U, Ramachandran S, da Silva Dias PL, Wofsy SC, Zhang X, 2007. Couplings between changes in the climate system and biogeochemistry. Climate Change 2007: The Physical Science Basis. Contribution of Working Group I to the Fourth Assessment Report of the Intergovernmental Panel on Climate Change; Cambridge (UK) and New York (NY): Cambridge University Press.

EEA (European Environment Agency). 2015. Air quality in Europe - 2015 report. Copenhagen. EEA Report. No.5/2015. 1977-8449, 64.

Eid MM, Saber A, El-Hussainy FM, Hassanein MK. 2014. Study the effect of emitted gases from the used fertilizers on some meteorological elements in Egypt. Nat Sci. 12 (12):133–147.

Elguindi N, Bi X, Giorgi F, Nagarajan B, Pal JS, Solmon F, Rauscher S, Zakey AO, Brien T, Nogherotto R, et al. 2014. Regional climate model RegCM:ICTP, Italy, reference manual version 4, 5.

El-Metwally M, Alfaro SC, Abdel Wahab M, Chatenet B. 2008. Aerosol characteristics over urban Cairo: seasonal variations as retrieved from Sunphotomete measurements. Geophys Res. 113:14219. doi:10.1029/2008JD009834.

El-Metwally M, Alfaro WMMA, Zakey AS, Chatenet B. 2011. Seasonal and inter-annual variability of the aerosol content in Cairo (Egypt) deduced from the comparison of MODIS aerosol retrievals with direct AERONE measurements. Atmos Res. 97:14–25.

Emmons LK, Walters S, Hess PG, Lamarque JF, Pfister GG, Fillmore D, Granier C, Guenther A, Kinnison D, Laepple T, et al. 2010. Description and evaluation of the model for ozone and related chemical tracers, version 4 (MOZART-4). Geosci Model Dev. 3:43–67. doi:10.5194/gmd-3-43-2010.

EPA (Environmental Protection Agency). 2010. Decontamination research and development conference. Washington (DC): U.S. Environmental Protection Agency. EPA/600/R, 11, 052-2011.

EPA (United States Environmental Protection Agency). 2018. Strengthens ozone standards to protect public health/Science-based standards to reduce sick days, asthma attacks, emergency room visits, greatly outweigh costs. Yosemite.epa.gov. 10(1):20. January 11.

Fetouh Y, El Askary H, El Raey M, Allali M, Sprigg WA, Kafatos M. 2013. Annual patterns of atmospheric pollutions and episodes over cairo Egypt. Adv Meteorol. 11:984.

Fountoukis C, Nenes A. 2007. A computationally efficient aerosol thermodynamic equilibriummodel forK+, Ca2+, Mg2+, NH4+, Na+, SO42−, NO3 −, Cl−, H2O aerosols. Atmos Chem Phys. 7:4639–4659. doi:10.5194/acp-7-4639-2007.

Giorgi F, Coppola E, Solmon F, Mariotti L, Sylla MB, Bi X, Elguindi N, Diro GT, Nair V, Giuliani G, et al. 2012. RegCM4: model description and preliminary tests over multiple CORDEX domains. Clim Res. 52:7–29. doi:10.3354/cr01018.

Grell GA. 2011. Prognostic evaluation of assumptions used by cumulus parameterizations. Mon Weather Rev. 121:764–787. doi:10.1175/1520-0493(1993)121<0764:PEOAUB>2.0.CO;2.

Grell GA, Peckham SE, Schmitz R, McKeen SA, Frost G, Skamarock WC, Eder B. 2005. Fully coupled online

chemistry within the WRF model. Atmos Environ. 39:6957–6975. doi:10.1016/j.atmosenv.2005.04.027.
Haywood JM, Ramaswamy V, Soden BJ. 1999. Tropospheric aerosol climate forcing in clear-sky satellite observations over the oceans. Science. 283:1299–1303. doi:10.1126/science.283.5406.1299.
Herman JR, Celarier E. 1997. Earth's surface reflectivity climatology at 340–380 nm from TOMS data. J Geophys Res. 102:3–28. doi:10.1029/97JD02074.
Holtslag AAM, Boville BA. 1993. Local versus nonlocal boundary-layer diffusion in a global climate model. J Clim. 6:1825–1842. doi:10.1175/1520-0442(1993)006<1825:LVNBLD>2.0.CO;2.
Inness A, Baier F, Benedetti A, Bouarar I, Chabrillat S, Clark H, Clerbaux C, Coheur P, Engelen RJ, Errera Q, et al.; MACC team. 2013. The MACC reanalysis: an 8 yr data set of atmospheric composition. Atmos Chem Phys. 13:4073–4109. doi:10.5194/acp-13-4073-2013.
IPCC (Intergovernmental Panel on Climate Change), 2013. Climate change 2013: the physical science basis. Contribution of Working Group I to the Fifth Assessment Report. Stocker, TF, D Qin, GK Plattner, M Tignor, SK Allen, J Boschung, A Nauels, Y. Xia.
Kiehl JT, Hack JJ, Bonan GB, Boville BA, Briegleb BP, Williamson DL, Rasch PJ. 1996. Description of the NCAR Community Climate Model (CCM3). Univ Corporation Atmos Res. 420:5065–6399.
Kok JF. 2011. A scaling theory for the size distribution of emitted dust aerosols suggests climate models underestimate the size of the global dust cycle. PNAS.18 (3):108–1016. January.
Lelieveld J, Gromov S, Pozzer A, Taraborrelli D. 2016. Global tropospheric hydroxyl distribution, budget and reactivity. Atmos Chem Phys. 16(19):12477. doi:10.5194/acp-16-12477-2016.
Lelieveld J, Klingmüller K, Pozzer A, Burnett RT, Haines A, Ramanathan V. 2019. Effects of fossil fuel and total anthropogenic emission removal on public health and climate. Proc Natl Acad Sci U S A. 116(15):7192–7197. doi:10.1073/pnas.1819989116.
Logan JA. 1985. Tropospheric ozone: seasonal behavior, trends, and anthropogenic influence. J Geophys Res. 90:24–541. doi:10.1029/JD090iD06p10463.
Madronich S, Flocke S. 1999. The role of solar radiation in atmospheric chemistry. In: Boule P, editor. Handbook of environmental chemistry. New York: Springer. p. 1–26.
Milford J, Gao D, Sillman S, Blossey P, Russell AG. 1994. Total reactive nitrogen (NOy) as an indicator for the sensitivity of ozone to NOx and hydrocarbons. J Geophys Res. 99:3533–3542. doi:10.1029/93JD03224.
Miranda J, Ferreira C, Silveira H, Relvas L, Duque P, Roebeling M, Lopes S, Costa A, Monteiro C, Gama E. 2016. A cost-efficiency and health benefit approach to improve urban air quality. Teixeira-Sci Total Environ. 569(570):342–345.
Mostafa AN, Zakey AS, Monem AS, Wahab MMA. 2018. Analysis of the surface air quality measurements in the Greater Cairo (Egypt) metropolitan. Global J Adv Res. 5 (6):207–214.
Mostafa AN, Zakey AS, Monem AS, Wahab MMA. 2019. Validation of RegCM-CHEM4 model by comparison with surface measurements in the Greater Cairo (Egypt) megacity. Environ Sci Pollut Res. 11356(19):05370.
Nenes A, Pandis SN, Pilinis C. 1998. A new thermodynamic equilibrium model for multiphase multicomponent inorganic aerosols. Aquat Geochem. 4:123–152. doi:10.1023/A:1009604003981.
NRC (National Research Council). 2001. Global air quality: an imperative for long-term observational strategies. Washington (DC): National Academy Press.
Ojumu AM, Abiodun BJ, Jenner S, Ojumu TV. 2013. Transport of atmospheric NOx and HNO3 over Cape Town. Atmos Chem Phys. 5:11827–11862.
Park M, Randel WJ, Emmons LK, Livesey NJ. 2009. Transport pathways of carbon monoxide in the Asian summer monsoon diagnosed from Model of Ozone and Related Tracers (MOZART). J Geophys Res. 114(8):1–11. doi:10.1029/2008JD010621.
Placet M, Mann CO, Gilbert RO, Niefer M. 2000. Emissions of ozone precursors from stationary sources: a critical review. Atmos Environ. 34:12–14. doi:10.1016/S1352-2310(99)00464-1.
Popescu F, Ionel I. 2010. Anthropogenic air pollution sources, air quality. Kumar A, editor. InTech. ISBN: 978-953-307-131-2. http://www.intechopen.com/books/airquality/
Putaud JP, Raes F, Van Dingenen R, Brüggemann E, Facchini MC, Decesari S, Fuzzi S, Gehrig R, Huglin C, Laj P, et al. 2010. European aerosol phenomenology-2: chemical characteristics of particulate matter at kerbside, urban, rural and background sites in Europe. Atmos Environ. 38:2579–2595. doi:10.1016/j.atmosenv.2004.01.041.
Robaa SM. 2004. A study of ultraviolet solar radiation at Cairo urban area, Egypt. Solor Energy. 77:251–259. doi:10.1016/j.solener.2004.01.008.
Roelofs RR, Laat ATJ, Lelieveld J, Dickerson GJ, Lobert JM. 2005. Source analysis of carbon monoxide pollution during INDOEX 1999. J Geophys Res. 16(28):481–495.
Saber A, Abdallah AA, Abdel Basset H, Eid MM, El-Hussainy FM. 2017. Statistical study of the aerosols emission over Egypt. Al Azhar Bull Sci. p. 63–80. 9. March.
Schultz M, Rast S, van Het Bolscher M, Pulles T, Brand R, Pereira J, Mota B, Spessa A, Dalspren S, van Nojie T, et al. 2005. Emission data sets and methodologies for estimating emissions. Max Planck institute for meteorology. Atmos Chem Phys. 15:2073–3109.
Shalaby A, Zakey AS, Tawfik AB, Solmon F, Giorgi F, Stordal F, Sillman S, Zaveri RA, Steiner AL. 2012. Implementation and evaluation of online gasphase chemistry within a regional climate model (RegCM-CHEM4). Geosci Model Dev. 5:741–760. doi:10.5194/gmd-5-741-2012.
Sillman S, He D. 2002. Some theoretical results concerning O3- NOx-VOC chemistry and NOx-VOC indicators. J Geophys Res. 107:22–4659. doi:10.1029/2001JD001123.
Sillman S, Samson PJ, Masters JM. 1995. Ozone formation in urban plumes transported over water: photochemical model and case studies in the Northeastern and Midwestern US. J Geophys Res. 98:12687–12699. doi:10.1029/93JD00159.
Solmon F, Giorgi F, Liousse C. 2016. Aerosol modelling for regional climate studies: 2006. application to anthropogenic particles and evaluation over a European/African do - main. Tellus B Chem Phys Meterol. 58:51–72.
Steiner A, Tawfik B, Shalaby A, Zakey AS, Abdel-Wahab MM, Salah Z, Solmon F, Sillman S, Zaveri RA. 2014. Climatological simulations of ozone and atmospheric aerosols in the Greater Cairo region. Clim Res. 59:207–228. doi:10.3354/cr01211.
Stevenson DS, Doherty RM, Sanderson MG, Johnson CE, Collins WJ, Derwent RG. 2005. Impacts of climate change and variability on tropospheric ozone and its precursors. Faraday Discuss. 130:41–57. doi:10.1039/b417412g.
Sylla MB, Coppola E, Mariotti L, Giorgi F, Ruti Aquila A, Bi X. 2009. Multiyear simulation of the African climate

using a regional climate model 56 (RegCM3) with the high resolution ERA-interim reanalysis. Clim Dyn. 35 (1):231–247. doi:10.1007/s00382-009-0613-9.

Vautard R, Honore C, Beekmann M, Rouil L. 2005. Simulation of ozone during the August 2003 heat wave and emission control scenarios. Atmos Environ. 39:2957–2967. doi:10.1016/j.atmosenv.2005.01.039.

Velchev K, Cavalli F, Hjorth J, Marmer E, Vignati E, Dentener F, Raes F. 2011. Ozone over the Western Mediterranean Sea – results from two years of shipborne measurements. Atmos Chem Phys. 11:675–688. doi:10.5194/acp-11-675-2011.

Wang Q, Wang Z, Zhang H. 2017. Impact of anthropogenic aerosols from global, East Asian, and non-EastAsian sources on East Asian summer monsoon system. Atmos Res. 183:224–236. doi:10.1016/j.atmosres.2016.08.023.

Wesely ML. 1989. Parameterization of surface resistance to gaseous dry deposition in regional-scale numerical models. Atmos Environ. 23:1293–1304. doi:10.1016/0004-6981(89)90153-4.

Wheida A, Nasser A, ElNazer M, Borbon A, Abo El Ata GA, Abdel Wahab M, Alfaro SC. 2017. Tackling the mortality from longterm exposure to outdoor air pollution in megacities: lessons from the Greater Cairo case study. Environ Res. 160:223–231. doi:10.1016/j.envres.2017.09.028.

WHO (World Health Organization). 2018. Ambient (outdoor) air quality and health. May. https://www.who.int/news-room/fact sheets/detail/ambient-(outdoor)-air-quality-and-health

WMO (World Meteorological Organization). 1995. Annual report 1994. Geneva (Switzerland): Secretariat of the World Meteorological rganization. ISBN: 978-92-63-10814-2.

IPCC. 2007. Climate Change 2007: The Physical Science Basis. Contribution of Working Group I to the Fourth Assessment Report of the Intergovernmental Panel on Climate Change. In: SolomonS, QinD, Manning M, Chen Z, MarquisM, Averyt KB, TignorM, Miller HL, editors. United Kingdom and New York: Cambridge University Press; p.996.

World Bank. 2013. The Arab republic of Egypt for better or for worse: air pollution in Greater Cairo. World Bank Annual Report, Report No. 73074-EG.

Zakey AS, Solmon F, Giorgi F. 2006. Implementation and testing of a desert dust module in a regional climate model. Atmos Chem Phys. 6:4687–4704. doi:10.5194/acp-6-4687-2006.

Zaveri R, Peters LK. 1999. A new lumped structure photochemical mechanism for large-scale applications. J Geophys Res. 104:30387–30415. doi:10.1029/1999JD900876.

Zeba N, Khokhara MF, Pozzerb A, Khanc SA. 2019. Exploring the temporal trends and seasonal behaviour of tropospheric trace gases over Pakistan by exploiting satellite observations. Atmos Environ. 198:279–290. doi:10.1016/j.atmosenv.2018.10.053.

Zeng S, Zhang Y. 2017. The effect of meteorological elements on continuing heavy air pollution: A case study in the Chengdu area during the 2014 Spring festival. Atmosphere. 8(4):71. doi:10.3390/atmos8040071.